ACS APPLIED MATERIALS & INTERFACES

Research Article

www.acsami.org

# In Situ Growth of Hollow Gold–Silver Nanoshells within Porous Silica Offers Tunable Plasmonic Extinctions and Enhanced Colloidal Stability

Chien-Hung Li,[†] Andrew C. Jamison,[†] Supparesk Rittikulsittichai,[†] Tai-Chou Lee,[‡] and T. Randall Lee*[,†]

[†]Department of Chemistry and the Texas Center for Superconductivity, University of Houston, 4800 Calhoun Road, Houston, Texas 77204-5003, United States

[‡]Department of Chemical and Materials Engineering, National Central University, 300 Jhongda Road, Jhongli City 32001, Taiwan

Supporting Information

**ABSTRACT:** Porous silica-coated hollow gold–silver nanoshells were successfully synthesized utilizing a procedure where the porous silica shell was produced prior to the transformation of the metallic core, providing enhanced control over the structure/composition of the bimetallic hollow core. By varying the reaction time and the precise amount of gold salt solution added to a porous silica-coated silver-core template solution, composite nanoparticles were tailored to reveal a readily tunable surface plasmon resonance that could be centered across the visible and near-IR spectral regions (~445–800 nm). Characterization by X-ray photoelectron spectroscopy, energy-dispersive X-ray spectroscopy, scanning electron microscopy, and transmission electron microscopy revealed that the synthetic methodology afforded particles having uniform composition, size, and shape. The optical properties were evaluated by absorption/extinction spectroscopy. The stability of colloidal solutions of our composite nanoparticles as a function of pH was also investigated, revealing that the nanoshells remain intact over a wide range of conditions (i.e., pH 2–10). The facile tunability, enhanced stability, and relatively small diameter of these composite particles (~110 nm) makes them promising candidates for use in tumor ablation or as photothermal drug-delivery agents.

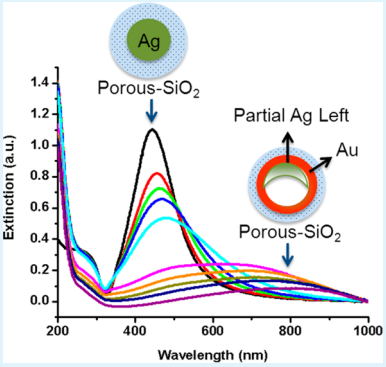


**KEYWORDS:** *hollow nanoshells, tunable plasmon, silica-coated, gold–silver, bimetallic*

## INTRODUCTION

Noble metal nanoparticles display a strong surface plasmon resonance (SPR) in which the frequency of incident photons is in resonance with the collective oscillation of the conduction band electrons at the surface of the metal.[1] Due to SPR, these nanoparticles can be designed to provide a strong light absorption that characteristically peaks within a broad range of wavelengths from the UV to the near-infrared, depending on the nature of the metal and the size and geometry of the particle.[2] For gold nanospheres, the SPR peak appears at ~520–640 nm, depending on the particle size,[3] while that for silver nanospheres falls in the range of ~390–460 nm.[4] Metal nanoshells are unique nanoparticle structures that have received a significant amount of attention because their tunable SPR bands have provided an additional means of targeting efficient light absorption and scattering. For example, the SPR peak position of gold nanoshells having a silica core and diameters less than 200 nm can be shifted from 600 to 1000 nm by simply varying the shell wall thickness and core size.[5] This ability to tune the SPR by designing nanoshells to absorb and scatter specific wavelengths of electromagnetic radiation allows researchers to target a specific window of absorption or scattering, depending on the desired application. Examples of how this type of tunability has proven useful can be found in the irradiation of subcutaneous nanoshells and nanorods by near-IR (NIR) wavelengths, which can penetrate into human tissue and cause little or no direct damage to the human body (~800–1300 nm).[5]

While the absorption/scattering characteristics of these particles can be used to produce effective contrast agents for imaging, the heat associated with SPR absorption can be used in photothermal therapeutics (e.g., tumor ablation or drug delivery).[5−8] Consequently, nanoparticles that absorb or scatter in the near-IR have received considerable attention due to their potential use in biomedical applications.[9,10] Importantly, the bioavailability of nanoparticles generally increases with decreasing size;[11] however, strategies for producing small gold nanoshells having NIR extinctions are relatively rare.[12−14]

In 2011, Vongsavat et al. demonstrated a two-step synthesis procedure for the fabrication of hollow gold–silver nanoshells having diameters that ranged from 40 to 100 nm.[15] According to this protocol, the hollow nanoshells were derived from silver nanoparticles that were synthesized by the reduction of silver nitrate using sodium citrate. The resulting silver particles were

Received: August 12, 2014
Accepted: October 16, 2014
Published: October 16, 2014

  

then used as templates to produce hollow gold−silver nanoshells via galvanic replacement by the addition of a gold salt solution to the nanoparticle solution. By varying the addition conditions (i.e., amount of gold salt solution and exposure time), the authors showed that the content of gold in the nanoshells can be adjusted along with the position of the SPR band, providing a means of tuning the absorption of light across the visible and into the NIR range.[15] The study also provided useful data showing the relationships between particle size, metal content, and the SPR band position. Notably, potential applications of these types of nanostructures are described in recent studies of similar hollow gold nanoshells that are being successfully employed in photothermal therapies.[16,17]

Nevertheless, unmodified hollow gold−silver nanoshells, like many uncoated (nonpassivated) metal nanostructures, are prone to agglomeration/precipitation.[18] One commonly used approach for applications in vivo that generally addresses this concern has been to encapsulate the nanoparticles in a coating of polyethylene glycol (PEG). However, Goodman et al. recently reported that PEG-coated hollow gold−silver nanoshells are unstable under acidic conditions, and also subject to decomposition in vivo.[19] This research team studied both uncoated and PEG-coated hollow gold−silver nanoshells, testing these samples under various pH conditions (pH = 2−10) for 24 h. Their studies found that these specialty nanoshells broke apart at low pH, even when the nanoshells were protected with PEG coatings.

Numerous alternative strategies for stabilizing nanoparticles are known.[18,20] One popular approach used in nanoparticle-based drug-delivery applications involves encapsulating the metal surfaces within a thin layer of silica—a shell that typically produces a negatively charged surface in aqueous media,[18,21,22] thereby enhancing colloidal stability by electrostatic means.[23] Importantly, silica nanoparticles show low systemic toxicity when capped with a variety of agents (e.g., polyvinylpyrrolidone, PVP) and even when uncoated in aggregate form.[24,25] Importantly, the surface of silica can be easily modified by various functional groups using conventional silane chemistry, providing a means of further passivating the surface and enabling a variety of applications.[26−28] A dense silica shell can, however, limit the access of small molecules and metal ions to the metal core. In contrast, encapsulation of the metal cores within porous silica shells enables penetration of these species through the shell while simultaneously inhibiting nanoparticle aggregation.[18,29,30]

We wished to use this approach to fabricate silica-coated gold−silver nanoshells with tunable extinctions and enhanced colloidal stability in aqueous solution, with the ultimate goal of using them for photothermal ablation or drug delivery.[5−8] An example of a similarly structured composite nanoparticle can be found in the work of Soulé et al.,[31] who prepared mesoporous silica-coated hollow gold−silver nanoshells using a sol−gel surfactant-templating method in which the bimetallic nanoshell cores were generated prior to the growth of the silica shell. Importantly, the composite diameter of the nanoshells in these pioneering studies was ∼300 nm, which is too large for many biomedical applications. Specifically, particles with diameters of 100−200 nm exhibit the greatest potential for prolonged circulation in the human body because they are large enough to avoid uptake by the liver and small enough to avoid filtration by the spleen.[32]

For the current investigation, we used a new procedure in which a porous silica coating modulates the overall size and interfacial structure of the resulting encapsulated composite nanoshells and affords precise control over the exposure of the precursor silver nanoparticle cores to a reactive gold salt solution, providing a facile means of tuning the position of the SPR band by controlling the extent of the galvanic reaction. We also compared the results from this new synthesis route to those obtained using the alternative synthesis strategy in which the gold−silver core is formed before coating with silica.[31] As a whole, the comparison shows that the hollow gold−silver nanoshells produced via the new procedure exhibit enhanced uniformity in size and shape. Additionally, we found that the silica layer protected the hollow gold−silver nanoshells from decomposition over a wide range of pH conditions, enabling their use in nanomedicinal applications ranging from diagnostic imaging to photothermal therapeutics.

## EXPERIMENTAL SECTION

**Materials.** Silver nitrate ($AgNO_3$; Aldrich), trisodium citrate dihydrate (NaCit; EM Science), potassium carbonate ($K_2CO_3$; Aldrich), hydrogen tetrachloroaurate(III) hydrate ($HAuCl_4 \cdot H_2O$; Strem), nitric acid ($HNO_3$; EM Science), hydrochloric acid (HCl; EM Science), ammonium hydroxide ($NH_4OH$; EM science), sodium hydroxide (NaOH; EM Science), tetraethylorthosilicate (Aldrich), and polyvinylpyrrolidone (PVP, MW ∼55,000; Aldrich) were purchased from the indicated suppliers and used without modification. Water was purified to a resistance of 18 MΩ (Academic Milli-Q Water System; Millipore Corp.) and filtered using a 0.22 μm filter. All glassware used in the experiments were cleaned in an aqua regia solution (3:1 HCl/$HNO_3$) and dried in the oven prior to use.

**Preparation of Silver Nanoparticle Cores.** Silver nanoparticles were prepared by one of the methods of Lee and Meisel that involves the reduction of $AgNO_3$ by sodium citrate.[33] An aliquot of $AgNO_3$ (0.0167 g, 0.100 mmol) was dissolved in 100 mL of $H_2O$. The solution was brought to reflux, and then 2 mL of 1% trisodium citrate solution was added under vigorous stirring. The solution was allowed to reflux for 30 min. A yellow-green colored solution was formed, consistent with the presence of silver nanoparticles. The solution was allowed to cool to room temperature (rt) and then centrifuged at 6000 rpm for 20 min before the supernatant was removed. This residue was rinsed twice with water. The aqueous solution containing the redispersed nanoparticles was then passed through a 0.2 μm PET syringe filter. This procedure generated monodisperse silver nanoparticles whose sizes can be adjusted from 40 to 100 nm, depending on the concentration of the reactants.

**Preparation of Porous Silica-Coated Silver Nanoparticles.** Two distinct steps were used to prepare porous silica-coated silver nanoparticles (Ag@porous $SiO_2$ NPs). The first step involved coating the silver nanoparticle cores with silica using an adaptation of the procedure used by Stöber et al. to prepare monodisperse silica nanoparticles.[34] In this process, 10 mL of silver nanoparticle solution were mixed with ammonium hydroxide (2 mL) and ethanol (22 mL). Under vigorous stirring, 25 μL of TEOS was added to this solution. The mixture was then further stirred overnight at rt to allow the silver cores to be encapsulated by the silica shells. The solution was then centrifuged at 4000 rpm for 20 min, and the isolated particles were redispersed in 20 mL of water. The centrifugation and redispersion steps were repeated five times, leading to the isolation of the silver nanoparticles coated with silica (Ag@$SiO_2$ NPs).

The second step involved coating the Ag@$SiO_2$ NPs with PVP followed by etching to form the porous shell, as reported by Zhang et al.[29] This process leads to porous silica having average pore sizes that range from 2.4 to 5.6 nm, depending upon the etching time.[29,30] In this process, the Ag@$SiO_2$ NP solution was mixed with 0.5 g PVP under sonication for 30 min and then refluxed at 90 °C for 3 h to form PVP-protected silica-coated silver nanoparticles (Ag@$SiO_2$−PVP NPs). After cooling the solution to rt, 0.4 mL of 1% NaOH solution

was added to the mixture to initiate the etching process, and the mixture was then stirred vigorously for 2 h. The resulting particles were purified by centrifugation at 4000 rpm for 20 min followed by redispersion in water. The centrifugation and redispersion steps were then repeated five times.

**Preparation of Porous Silica-Coated Hollow Gold−Silver Nanoshells.** To produce the final porous silica-coated hollow gold−silver nanoshells (Au−Ag@porous $SiO_2$ nanoshells), a basic solution of gold salt (K−gold solution) was prepared using the method reported by Oldenburg et al.[35] Specifically, 0.025 g of potassium carbonate ($K_2CO_3$) was added to 100 mL of Milli-Q water, which was then infused with 2 mL of 1% $HAuCl_4 \cdot H_2O$ solution. The mixture, which was initially yellow in color, became colorless 30 min after the reaction was initiated. The flask was then covered with aluminum foil to shield it from light, and the solution was stored in a refrigerator overnight.

To determine the best parameters for producing the final composite particles, we added defined aliquots of the K−gold solution to a defined amount of the Ag@porous $SiO_2$ NP solution. Each solution was continuously stirred, and the SPR band was monitored over time by UV−visible (UV−vis) spectroscopy until the SPR band stopped shifting to longer wavelengths. The results reported herein started with ∼2 mL aliquots of Ag@porous $SiO_2$ NP solution placed in several small vials that each contained a small stirring bar. A ∼2 mL aliquot of K−gold solution was added to each of the vials, and the mixture was vigorously stirred. The resulting mixture was purified by centrifugation at 4000 rpm for 20 min, and the supernatant was then decanted. Milli-Q water was added, and the centrifugation and decantation steps were repeated two more times. The isolated composite particles were redispersed in water prior to characterization.

**Characterization Methods.** The morphology of the obtained particles was evaluated using a LEO-1525 scanning electron microscope (SEM) operating at an accelerating voltage of 15 kV. To obtain high-resolution SEM images, all samples were deposited on silicon wafers. Similarly, the size and morphology of the particles were evaluated by employing a JEM-2000 FX transmission electron microscope (TEM) operating at an accelerating voltage of 200 kV. All TEM samples were deposited on 300 mesh holey carbon-coated copper grids and dried overnight before analysis. Energy-dispersive X-ray spectroscopy (EDX) measurements were collected using an Oxford EDX attached to the TEM microscope. X-ray photoelectron spectroscopy (XPS) spectra were collected using a PHI 5700 XPS instrument equipped with monochromatic Al K$\alpha$ X-ray source. The XPS-derived atomic concentration was calculated by standard XPS processing software (Multipak). UV−vis spectra were obtained using a Cary 50 Scan UV−visible spectrometer over the wavelength range of 200−1000 nm.

**Photothermal Studies.** To explore the potential use of the nanoparticles in photothermal treatment applications, 3.0 mL aliquots of the porous silica-coated hollow gold−silver nanoshell solution were loaded in quartz cuvettes and irradiated by a diode laser (AixiZ, CW 300 mW, 808 ± 10 nm) at a power density of ∼5 $Wcm^{-2}$ for 10 min. During the course of irradiation, the temperature of the suspension was measured at 1 s intervals using a fiber optic temperature sensor (Neoptix) with a temperature resolution of 0.1 °C. After exposure, the spectrum of the nanoshells was immediately collected (within 30 s).

**pH Stability Studies.** The pH of the colloidal solutions was adjusted using 0.1 M solutions of HCl and NaOH to obtain the desired value (i.e., 2, 3, 4, 6, 8, 10), and was measured with a pH meter and pH test paper (Whatman). Glass sample vials were prepared for each pH-adjusted colloidal solution (3.5 mL), along with the unadjusted standard (pH 7), and placed on a Vari-Mix Test Tube Rocker for 24 h. After 24 h, the optical properties of the composite nanoshells were measured by UV−vis spectroscopy, and then the particles were separated from their supernatant by centrifugation at 4000 rpm for 20 min followed by redispersion in water for further characterization.

## RESULTS AND DISCUSSION

**Synthetic Strategy.** The strategy used to prepare our porous silica-coated hollow gold−silver nanoshells is illustrated in Scheme 1. For comparison, the results obtained via an alternative strategy involving the formation of the hollow Au−Ag nanoshell followed by coating with porous silica are provided in the Supporting Information.

**Scheme 1. Strategy for the Synthesis of Porous Silica-Coated Hollow Gold−Silver Nanoshells**

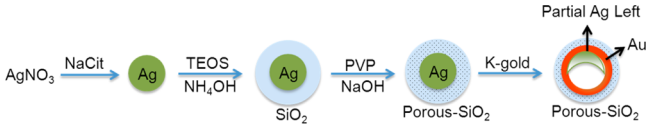


This visual summary of the formation of the bimetallic hollow nanoshells provides perspective regarding the potential of this methodology. The first step centers on the synthesis of monodisperse silver nanoparticles. The second step involves coating the silver nanoparticles with a silica layer to prevent nanoparticle aggregation and enhance stability. The addition of PVP in the third step provides a coating that partially protects the silica surface from etching by base, effectively retarding the etching process and allowing the controlled formation of a porous silica surface as a function of time. Due to the presence of the porous silica shell, the subsequent addition of K−gold solution in the final step affords a gradual displacement of the silver core by galvanic replacement without affecting the silica overlayer. This route led to greater nanoparticle uniformity and improved morphological consistency than the alternative route described in the Supporting Information (Scheme S1 and Figure S1). Regarding the galvanic reaction, because the standard reduction potential of the $Au^{3+}/Au$ pair (0.99 V vs standard hydrogen electrode, SHE, for $AuCl_4$-) is higher than that of the $Ag^+/Ag$ pair (0.80 V vs SHE), Ag can be oxidized into $Ag^+$ when the silver nanostructures and the K−gold solution are in contact (eq 1),[36] and the gold salts can be reduced to $Au^0$, allowing the gold to blend into the metal shell structure.

$$3Ag + Au^{3+} \rightarrow 3Ag^+ + Au \quad (1)$$

**Size and Morphology of the Porous Silica-Coated Silver Nanoparticles.** Both SEM and TEM were used to follow the development of the morphologies and particle growth patterns of the silica-coated silver nanoparticles and porous silica-coated silver nanoparticles. Figure 1a,b shows uniform Ag@$SiO_2$ NP structures with a total diameter of 108 ± 10 nm and a shell thickness of ∼25 nm. After the addition of the NaOH solution to the Ag@$SiO_2$−PVP NP solution to initiate the etching process, the porous silica structure was formed. A prior report states that etching starts from the interior, where there is no interaction with the PVP coating, and extends to the outer surface.[29] Our images appear to show that the porosity of the silica shells is uniform. Further, when compared to the images in Figure 1, panels a and b, the images in panels c and d show that the porous silica NPs retain the shape and dimensions of the nonporous structures.

**Surface Composition of the Porous Silica-Coated Silver Nanoparticles.** XPS data show the surface composition of the Ag@$SiO_2$ NPs and the Ag@porous $SiO_2$ NPs (Table 1). The data are consistent with the anticipated presence of carbon,

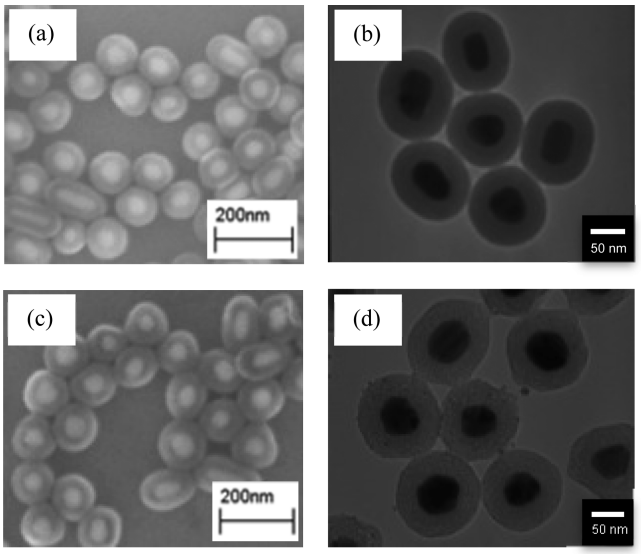


**Figure 1.** (a) SEM and (b) TEM images of the nonporous Ag@$SiO_2$ NPs; (c) SEM and (d) TEM images of the Ag@porous $SiO_2$ NPs.

**Table 1. XPS-Derived Atomic Composition of the Nanoparticles**

| | atomic concn (%)[a] | | | | | |
|---|---|---|---|---|---|---|
| sample | N | C | O | Si | Ag | Si/Ag ratio |
| Ag@$SiO_2$–PVP NPs (before etching) | 3 | 36 | 44 | 15 | 3 | 5 |
| Ag@$SiO_2$–PVP NPs (after etching) | 3 | 45 | 38 | 10 | 3 | 3 |

[a]Atomic concentrations were calculated in Multipak.

nitrogen, oxygen, silicon, and silver. Prior to etching, the Si/Ag ratio was 5:1. However, after the addition of the etchant, the Si/Ag ratio changed to 3:1. Based upon these data, we conclude there is a distinct reduction in silica content as a consequence of the etching process.

**Size and Morphology of the Porous Silica-Coated Hollow Gold–Silver Nanoshells.** Figure 2 shows both SEM and TEM images of the Au–Ag@porous $SiO_2$ nanoshells after subjecting the porous $SiO_2$-coated Ag nanoparticle cores to galvanic replacement for 24 h. These images reveal that the inner solid Ag core has been converted to a core/shell structure, a change that occurred upon adding the K–gold solution, where the gold ions underwent reaction with the

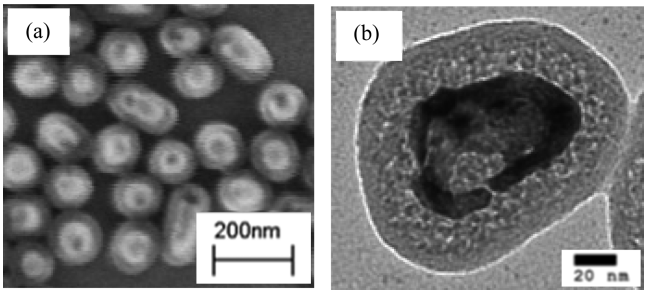


**Figure 2.** (a) SEM image of porous silica-coated hollow gold–silver nanoshells after 24 h of galvanic replacement; (b) TEM image of a single porous silica-coated hollow gold–silver nanoshell after 24 h of galvanic replacement.

metallic silver nanoparticle cores. At the same time, the Ag core was partially oxidized and dissolved into solution. The hollow morphology is particularly evident in Figure 2b.

**Composition of the Porous Silica-Coated Hollow Gold–Silver Nanoshells.** EDX data reveal the elemental composition of the Au–Ag@porous $SiO_2$ nanoshells after subjecting the porous $SiO_2$-coated Ag nanoparticle cores to galvanic replacement for 24 h. The spectrum in Figure 3 confirms the presence of gold (M$\alpha$ and L$\alpha$ peaks at 2.12 and 9.71 keV, respectively), silver (L$\alpha$ and L$\beta$ peaks at 3.05 and 3.20 keV, respectively), and silica (K$\alpha$ peak at 1.74 keV). Also, a copper peak is observed that is associated with the supporting copper grid used for analysis. Additionally, Table 2 shows the EDX-derived atomic composition of key atomic components of the nanoshells, along with the molar ratio of Ag to Au, which is 5.9:1.0.

**Optical Properties of the Porous Silica-Coated Hollow Gold–Silver Nanoshells.** Figure 4 shows the extinction spectra for the Au–Ag@porous $SiO_2$ nanoshells taken at various times during exposure of the Ag@porous $SiO_2$ nanoparticles to the K–gold solution. Before adding K–gold solution, the porous silica-coated silver nanoparticles exhibited a relatively sharp SPR peak at ~445 nm. After adding the K–gold solution, the SPR maximum shifted from ~445 nm up to ~800 nm, depending on the agitation time. After 24 h, the SPR band stopped shifting, which was taken to indicate that the bimetallic shells achieved a stable composition/structure. The observed red shift can be attributed to both the replacement of silver by gold and the generation of a metallic shell structure having a hollow dielectric core.[5,35] Prior studies of the formation of Au–Ag nanoshells or nanostructures (absent an overlying silica shell) have found that a thin layer of gold initially deposits on the surface of the silver core of the nanoparticle, followed by the oxidation of the silver core and its partial dissolution into the surrounding solution, forming a hollow structure.[37,38]

The broadness of the SPR band and its peak position depend not only on the metal content of the core, but also on the distribution of metal shell sizes and the thickness of the shell.[5,39] Importantly, our porous silica-coated hollow gold–silver nanoshells exhibit their maximum SPR peak in the NIR region upon completion of the formation of the shell/hollow core structure, which renders them attractive for use in various theranostic applications.[10,16,17,40]

**Photothermal Properties of the Porous Silica-Coated Hollow Gold–Silver Nanoshells.** Figure 5 provides insight into the photothermal properties of the Au–Ag@porous $SiO_2$ nanoshells. The composite nanoparticles were irradiated with a NIR laser emitting light at a wavelength of 808 nm. The temperature of the aqueous solution containing the porous silica-coated hollow gold nanoshells was measured at intervals of 30 s over a period of 10 min and increased from 24 to 36 °C over this time frame. These measurements reveal a potential for photothermal applications for such hollow bimetal nanoshell structures; moreover, the collective data suggests that the light-activated thermal response can be modulated by adjusting the time of exposure of the Ag@porous $SiO_2$ NPs to the K–gold solution.

**Stability of the Porous Silica-Coated Hollow Gold–Silver Nanoshells as a Function of pH.** Figure 6a illustrates the stability of the Au–Ag@porous $SiO_2$ nanoshells after 24 h of exposure under various pH conditions. Notably, the SPR peak at pH 10 (~770 nm) is slightly blue-shifted from our

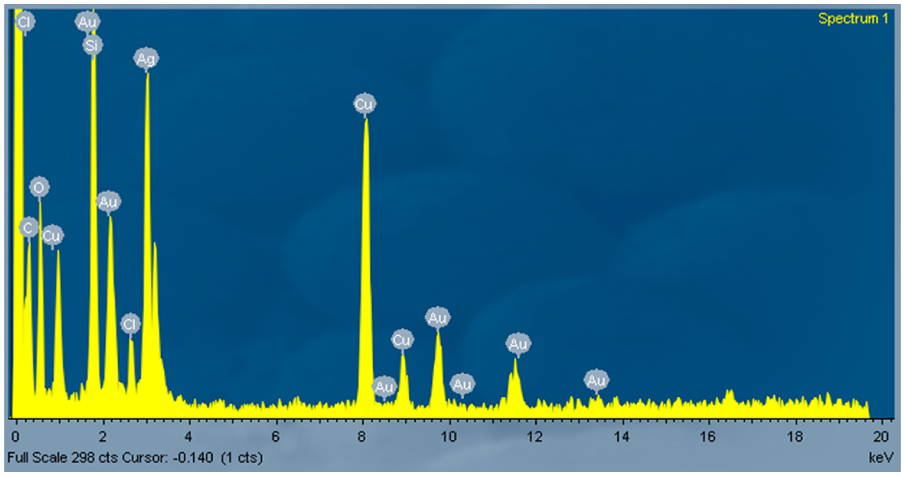


**Figure 3.** EDX of the porous silica-coated hollow gold–silver nanoshells after 24 h of galvanic replacement.

**Table 2. EDX-Derived Atomic Composition of the Nanoshells after 24 h of Galvanic Replacement**

| | weight (%) | | | | molar ratio |
|---|---|---|---|---|---|
| sample | Si | O | Ag | Au | Ag/Au |
| Au–Ag@porous $SiO_2$ nanoshells | 8 | 15 | 51 | 16 | 5.9 |

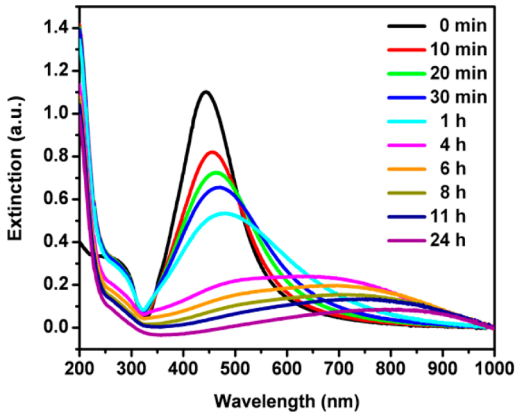


**Figure 4.** UV–vis spectra of porous silica-coated hollow gold–silver nanoshells as a function of the amount of time after adding K–gold solution to the Ag@porous $SiO_2$ NP solution.

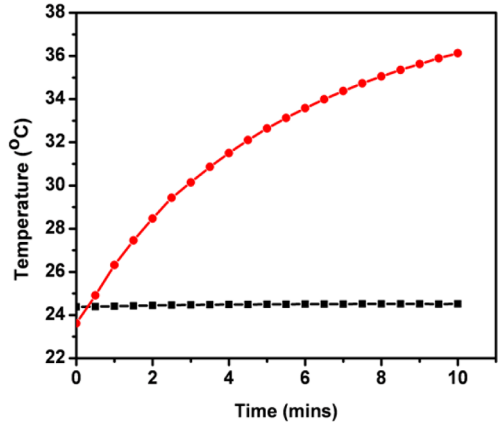


**Figure 5.** Temperature of aqueous solution containing silica-coated hollow gold–silver nanoshells developed by galvanic replacement for 24 h (red ●) and subsequently exposed to NIR laser irradiation. Measurements were collected at 30 s intervals over 10 min and compared to the response of pure water (■) upon exposure to the laser.

"standard" sample at pH 7 (~800 nm), which indicates that the nanoshells are largely robust up to pH 10. Furthermore, the observed blue shift probably reflects changes in the refractive index of the material surrounding the Au–Ag nanoshell core related to the partial dissolution of the silica shell under basic conditions.[41−43] With the loss of silica, small molecules such as water can penetrate the silica shell around the gold–silver nanoshell cores, changing the refractive index of the materials in contact with these cores.[44] For the materials involved, the refractive index of water is 1.33,[45] which is smaller than that of silica at 1.46.[46] However, Rayss et al. reported that the refractive index of a silica surface increases with an increase in the concentration of adsorbed cations.[47] Such an increase occurs with an increase in pH, and as the pH of the nanoshell solution is raised above pH 7, there is a notable increase in adsorbed cations. However, this effect is counter to the trend observed in our data and is apparently minimal compared to the change in the silica shell refractive index associated with the partial loss of silica from the shell via dissolution under mildly basic conditions.

In contrast, the extinction spectra for colloidal solutions over the range of pH 8 to pH 4 show a small red shift in peak position (from ~800 to ~820 nm, respectively). Notably, the observed red shift can be attributed to a decrease in the surface charge of the silica shell as the charge on these composite nanoparticles begins to approach the isoelectric point of silica (~pH 2).[48] Absent a sufficient charge to maintain particle separation, some of the particles are likely to form aggregates, causing the SPR peak to shift to slightly longer wavelengths.[49] Further, the intensity of the SPR bands for the nanoshell solutions at pH 2 and pH 3 decrease dramatically, and the peak positions are more noticeably red-shifted (by ~60 nm), which is consistent with a model in which the nanoshells aggregate and precipitate as the pH of the solution reaches the isoelectric point of silica.[48]

Importantly, for the sample held at pH 2 for 24 h, we subsequently increased the pH to 8 by adding mild base ($NH_4OH$) and observed that the extinction band substantially recovered to its original position and intensity (Figure 6b); similar behavior was observed for the sample held at pH 3 for


dx.doi.org/10.1021/am505424w | ACS Appl. Mater. Interfaces 2014, 6, 19943−19950

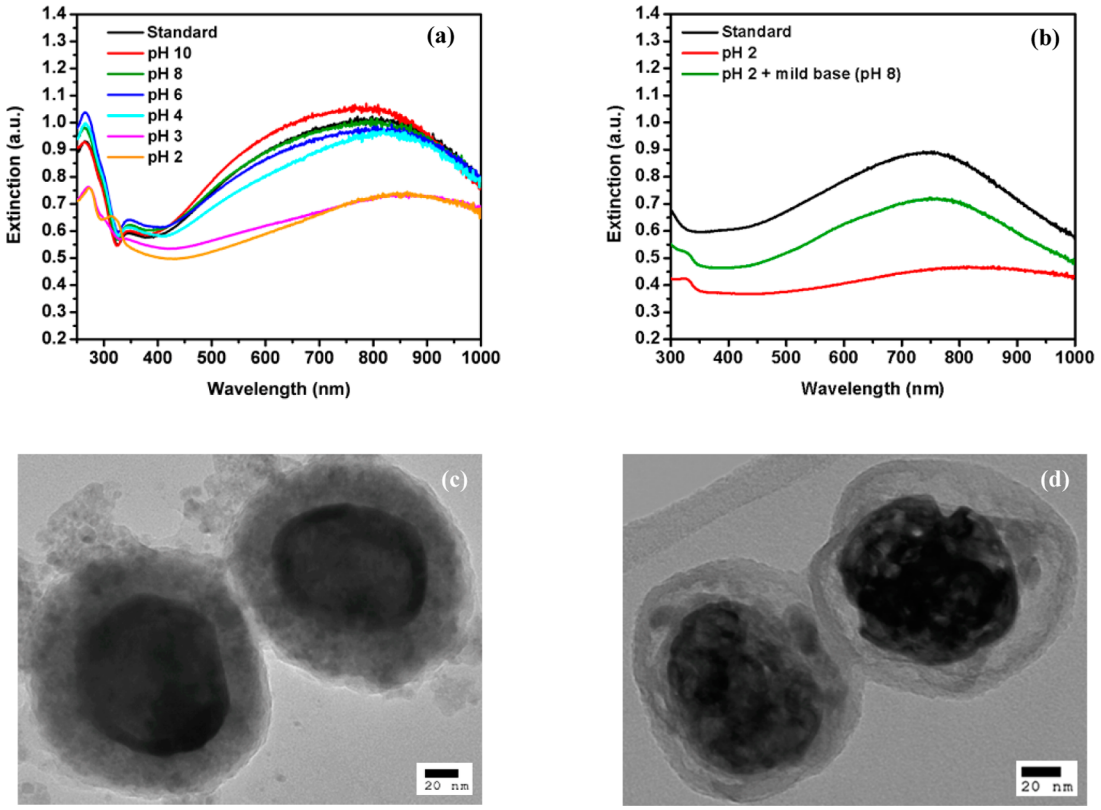


**Figure 6.** (a) UV–vis spectra of porous silica-coated hollow gold–silver nanoshell solutions upon exposure to various solution pH values for 24 h. (b) UV–vis spectra of porous silica-coated hollow gold–silver nanoshell solutions after 24 h at pH 2 before and after adding $NH_4OH$ to adjust the pH to 8. (c) TEM image of the porous silica-coated hollow gold–silver nanoshells after exposure to a solution at pH 2 for 24 h. (d) TEM image of the porous silica-coated hollow gold–silver nanoshells that were exposed to a pH 2 solution for 24 h and subsequently adjusted to pH 8 by adding $NH_4OH$. Each spectral plot includes a standard solution of the porous silica-coated hollow gold–silver nanoshells (pH 7) that was not subjected to any pH adjustment.

24 h (Supporting Information). These observations are consistent with a model in which the surface charge on the silica coatings was restored by the addition of mild base.[48,49] Additionally, the TEM images of the silica-coated nanoshells that were exposed to pH 2 for 24 h show that the Au–Ag nanoshells remain intact inside the porous silica shell coating (Figure 6c), in contrast to previously studied Au–Ag nanoshells having no silica coating.[19] Notably, the TEM images of these nanoshells after adjusting the solution to pH 8 show that they retain their shape and morphology (Figure 6d). Colloidal recovery studies of the nanoshells held at pH 3 for 24 h are provided in the Supporting Information.

## CONCLUSIONS

Porous silica-coated hollow gold–silver nanoshells (Au–Ag@porous $SiO_2$ nanoshells) with diameters of 108 ± 10 nm were synthesized and characterized by UV–vis, SEM, TEM, XPS, and EDX. The synthetic strategy used to prepare these composite nanoshells led to particles with greater uniformity when compared to those produced via an alternative route used to prepare similar composite particles. The optical properties of the composite nanoshells show that the most intense peak associated with the SPR band can shift from the visible to the NIR range (~445–800 nm) depending on the extent of exposure of the PVP-protected silica-coated silver nanoparticle cores to K–gold salt solution. Additionally, irradiation of an aqueous solution of the Au–Ag@porous $SiO_2$ nanoshells with a NIR laser (808 nm) generated sufficient heat to increase the temperature of the solution from 24 to 36 °C after 10 min of exposure to the beam, which indicates that they have a strong photothermal response, making them good candidates for nanomedicinal applications. This conclusion is further supported by the observation that these nanoshells remain intact in aqueous solution for 24 h over a wide range of pH conditions. These results, along with the tunability of the bimetallic nanoshell cores, should generate interest among researchers seeking versatile nanoparticles for projects such as targeted photothermal therapeutic treatments, light-activated drug-delivery release mechanisms, or photocatalysis reactions that are initiated by visible or NIR light.

## ASSOCIATED CONTENT

### Supporting Information

Detailed description of the synthetic procedure for the alternative strategy, along with an illustration of this strategy; SEM and TEM images of the resulting composite particles. This material is available free of charge via the Internet at http://pubs.acs.org.

## AUTHOR INFORMATION

### Corresponding Author

*E-mail: trlee@uh.edu.

### Notes

The authors declare no competing financial interest.

## ■ ACKNOWLEDGMENTS

The Asian Office of Aerospace Research and Development (AFOSR/AOARD 134032), the Robert A. Welch Foundation (Grant No. E-1320), and the Texas Center for Superconductivity at the University of Houston provided generous support for this research.

## ■ REFERENCES

(1) Kreibig, U.; Vollmer, M. E. *Optical Properties of Metal Clusters*, Vol. 25, Springer-Verlag: Berlin, 1995.
(2) Kelly, K. L.; Coronado, E.; Zhao, L. L.; Schatz, G. C. The Optical Properties of Metal Nanoparticles: The Influence of Size, Shape, and Dielectric Environment. *J. Phys. Chem. B* **2003**, *103*, 668−677.
(3) Ziegler, C.; Eychmüller, A. Seeded Growth Synthesis of Uniform Gold Nanoparticles with Diameters of 15−300 nm. *J. Phys. Chem. C* **2011**, *115*, 4502−4506.
(4) Agnihotri, S.; Mukherji, S.; Mukherji, S. Size-Controlled Silver Nanoparticles Synthesized Over the Range 5−100 nm Using the Same Protocol and Their Antibacterial Efficacy. *RSC Adv.* **2014**, *4*, 3974−3983.
(5) Erickson, T. A.; Tunnell, J. W. Gold Nanoshells in Biomedical Applications. In *Nanomaterials for the Life Sciences*; Kumar, C. S. S. R., Ed.; Wiley-VCH Verlag GmbH & Co.: Weinheim, 2009; Vol. 3.
(6) Kim, J.-H.; Lee, T. R. Thermo-Responsive Hydrogel-Coated Gold Nanoshells for In Vivo Drug Delivery. *J. Biomed. Pharm. Eng.* **2008**, *2*, 29−35.
(7) Loo, C.; Lin, A.; Hirsch, L.; Lee, M.-H.; Barton, J.; Halas, N.; West, J.; Drezek, R. Nanoshell-Enabled Photonics-Based Imaging and Therapy of Cancer. *Technol. Cancer Res. Treat.* **2004**, *3*, 33−40.
(8) Hirsch, L. R.; Stafford, R. J.; Bankson, J. A.; Sershen, S. R.; Rivera, B.; Price, R. E.; Hazle, J. D.; Halas, N. J.; West, J. L. Nanoshell-Mediated Near-Infrared Thermal Therapy of Tumors under Magnetic Resonance Guidance. *Proc. Nat. Acad. Sci. U.S.A.* **2003**, *100*, 13549−13554.
(9) Xia, Y.; Li, W.; Cobley, C. M.; Chen, J.; Xia, X.; Zhang, Q.; Yang, M.; Cho, E. C.; Brown, P. K. Gold Nanocages: From Synthesis to Theranostic Applications. *Acc. Chem. Res.* **2011**, *44*, 914−924.
(10) Melancon, M. P.; Zhou, M.; Li, C. Cancer Theranostics with Near-Infrared Light-Activatable Multimodal Nanoparticles. *Acc. Chem. Res.* **2011**, *44*, 947−956.
(11) Liversidge, G. G.; Cundy, K. C. Particle Size Reduction for Improvement of Oral Bioavailability of Hydrophobic Drugs: I. Absolute Oral Bioavailability of Nanocrystalline Danazol in Beagle Dogs. *Int. J. Pharm.* **1995**, *125*, 91−97.
(12) Gobin, A. M.; Watkins, E. M.; Quevedo, E.; Colvin, V. L.; West, J. L. Near-Infrared-Resonant Gold/Gold Sulfide Nanoparticles as a Photothermal Cancer Therapeutic Agent. *Small* **2010**, *6*, 745−752.
(13) Schwartzberg, A. M.; Olson, T. Y.; Talley, C. E.; Zhang, J. Z. Synthesis, Characterization, and Tunable Optical Properties of Hollow Gold Nanoshperes. *J. Phys. Chem. B* **2006**, *110*, 19935−19944.
(14) Prevo, B. G.; Esakoff, S. A.; Mikhailovsky, A.; Zasadzinski, J. A. Scalable Routes to Gold Nanoshells with Tunable Sizes and Response to Near-Infrared Pulsed-Laser Irradiation. *Small* **2008**, *4*, 1183−1195.
(15) Vongsavat, V.; Vittur, B. M.; Bryan, W. W.; Kim, J.-H.; Lee, T. R. Ultrasmall Hollow Gold-Silver Nanoshells with Extinctions Strongly Red-Shifted to the Near-Infrared. *ACS. Appl. Mater. Interfaces* **2011**, *3*, 3616−3624.
(16) Melancon, M. P.; Lu, W.; Yang, Z.; Zhang, R.; Cheng, Z.; Elliot, A. M.; Stafford, J.; Olson, T.; Zhang, J. Z.; Li, C. In Vitro and In Vivo Targeting of Hollow Gold Nanoshells Directed at Epidermal Growth Factor Receptors for Photothermal Ablation Therapy. *Mol. Cancer Ther.* **2008**, *7*, 1730−1739.
(17) Lu, W.; Melancon, M. P.; Xiong, C.; Huang, Q.; Elliott, A.; Song, S.; Zhang, R.; Flores, L. G., II; Gelovani, J. G.; Wang, L. V.; Ku, G.; Stafford, R. J.; Li, C. Effects of Photoacoustic Imaging and Photothermal Ablation Therapy Mediated by Targeted Hollow Gold Nanospheres in an Orthotopic Mouse Xenograft Model of Glioma. *Cancer Res.* **2011**, *71*, 6116−6121.
(18) Mulvaney, P.; Liz-Marzán, L. M.; Giersig, M.; Ung, T. Silica Encapsulation of Quantum Dots and Metal Clusters. *J. Mater. Chem.* **2000**, *10*, 1259−1270.
(19) Goodman, A. M.; Cao, Y.; Urban, C.; Neumann, O.; Ayala-Orozco, C.; Knight, M. W.; Joshi, A.; Nordlander, P.; Halas, N. J. The Surprising in Vivo Instability of Near-IR-Absorbing Hollow Au-Ag Nanoshells. *ACS Nano* **2014**, *8*, 3222−3231.
(20) Srisombat, L.; Jamison, A. C.; Lee, T. R. Stability: A Key Issue for Self-Assembled Monolayers on Gold as Thin-Film Coatings and Nanoparticle Protectants. *Colloids Surf., A* **2011**, *390*, 1−19.
(21) Liz-Marzán, L. M.; Giersig, M.; Mulvaney, P. Synthesis of Nanosized Gold-Silica Core-Shell Particles. *Langmuir* **1996**, *12*, 4329−4335.
(22) Yu, T.; Malugin, A.; Ghandehari, H. Impact of Silica Nanoparticle Design on Cellular Toxicity and Hemolytic Activity. *ACS Nano* **2011**, *5*, 5717−5728.
(23) Metin, C. O.; Lake, L. W.; Miranda, C. R.; Nguyen, Q. P. Stability of Aqueous Silica Nanoparticle Dispersions. *J. Nanopart. Res.* **2011**, *13*, 839−850.
(24) Zhang, H.; Dunphy, D. R.; Jiang, X.; Meng, H.; Sun, B.; Tarn, D.; Xue, M.; Wang, X.; Lin, S.; Ji, Z.; Li, R.; Garcia, F. L.; Yang, J.; Kirk, M. L.; Xia, T.; Zink, J. I.; Nel, A.; Brinker, C. J. Processing Pathway Dependence of Amorphous Silica Nanoparticle Toxicity: Colloidal vs Pyrolytic. *J. Am. Chem. Soc.* **2012**, *134*, 15790−15804.
(25) Izak-Nau, E.; Kenesei, K.; Murali, K.; Voetz, M.; Eiden, S.; Puntes, V. F.; Duschl, A.; Madarász, E. Interaction of Differently Functionalized Fluorescent Silica Nanoparticles with Neural Stem- and Tissue-Type Cells. *Nanotoxicology* **2014**, *8*, 138−148.
(26) Yu, T.; Greish, K.; McGill, L. D.; Ray, A.; Ghandehari, H. Influence of Geometry, Porosity, and Surface Characteristics of Silica Nanoparticles on Acute Toxicity: Their Vasculature Effect and Tolerance Threshold. *ACS Nano* **2012**, *6*, 2289−2301.
(27) Haensch, C.; Hoeppener, S.; Schubert, U. S. Chemical Modification of Self-Assembled Silane Based Monolayers by Surface Reactions. *Chem. Soc. Rev.* **2010**, *39*, 2323−2334.
(28) Trewyn, B. G.; Slowing, I. I.; Giri, S.; Chen, H.-T.; Lin, V. S. -Y. Synthesis and Functionalization of a Mesoporous Silica Nanoparticle Based on the Sol-Gel Process and Applications in Controlled Release. *Acc. Chem. Res.* **2007**, *40*, 846−853.
(29) Zhang, Q.; Zhang, T.; Ge, J.; Yin, Y. Permeable Silica Shell through Surface-Protected Etching. *Nano Lett.* **2008**, *8*, 2867−2871.
(30) Zhang, Q.; Ge, J.; Goebl, J.; Hu, Y.; Lu, Z.; Yin, Y. Rattle-Type Silica Colloidal Particles Prepared by A Surface-Protected Etching Process. *Nano Res.* **2009**, *2*, 583−591.
(31) Soulé, S.; Allouche, J.; Dupin, J.-C.; Martinez, H. Design of Ag−Au Nanoshell Core/Mesoporus Oriented Silica Shell Nanoparticles through a Sol−Gel Surfactant Templating Method. *Microporous Mesoporous Mater.* **2013**, *171*, 72−77.
(32) Petros, R. A.; DeSimone, J. M. Strategies in the Design of Nanoparticles for Therapeutic Applications. *Nat. Rev. Drug Discovery* **2010**, *9*, 615−627.
(33) Lee, P. C.; Meisel, D. Adsorption and Surface-Enhanced Raman of Dyes on Silver and Gold Sols. *J. Phys. Chem.* **1982**, *86*, 3391−3395.
(34) Stöber, W.; Fink, A.; Bohn, E. Controlled Growth of Monodisperse Silica Spheres in the Micron Size Range. *J. Colloid Interface Sci.* **1968**, *26*, 62−69.
(35) Oldenburg, S. J.; Averitt, R. D.; Westcott, S. L.; Halas, N. J. Nanoengineering of Optical Resonances. *Chem. Phys. Lett.* **1998**, *288*, 243−247.
(36) Sun, Y.; Mayers, B.; Xia, Y. Metal Nanostructures with Hollow Interiors. *Adv. Mater.* **2003**, *15*, 641−646.
(37) Sun, Y.; Xia, Y. Mechanistic Study on the Replacement Reaction between Silver Nanostructures and Chloroauric Acid in Aqueous Medium. *J. Am. Chem. Soc.* **2004**, *126*, 3892−3901.
(38) Choi, Y.; Hong, S.; Liu, L.; Kim, S. K.; Park, S. Galvanically Replaced Hollow Au−Ag Nanospheres: Study of Their Surface Plasmon Resonance. *Langmuir* **2012**, *28*, 6670−6676.

(39) Hao, E.; Li, S.; Bailey, R. C.; Zou, S.; Schatz, G. C.; Hupp, J. T. Optical Properties of Metal Nanoshells. *J. Phys. Chem. B* **2004**, *108*, 1224−1229.
(40) Zhang, J. Z. Biomedical Applications of Shape-Controlled Plasmonic Nanostructures: A Case Study of Hollow Gold Nanospheres for Photothermal Ablation Therapy of Cancer. *J. Phys. Chem. Lett.* **2010**, *1*, 686−695.
(41) Alexander, G. B.; Heston, W. M.; Iler, R. K. The Solubility of Amorphous Silica in Water. *J. Phys. Chem.* **1954**, *58*, 453−455.
(42) Noguez, C. Surface Plasmons on Metal Nanoparticles: The Influence of Shape and Physical Environment. *J. Phys. Chem. C* **2007**, *111*, 3806−3819.
(43) Lee, S. H.; Jamison, A. C.; Hoffman, D. M.; Jacobson, A. J.; Lee, T. R. Preparation and Characterization of Polymeric Thin Films Containing Gold Nanoshells via Electrostatic Layer-by-Layer Self-Assembly. *Thin Solid Films* **2014**, *558*, 200−207.
(44) Zhang, L.; Blom, D. A.; Wang, H. Au-$Cu_2O$ Core-Shell Nanoparticles: A Hybrid Metal-Semiconductor Heteronanostructure with Geometrically Tunable Optical Properties. *Chem. Mater.* **2011**, *23*, 4587−4598.
(45) Li, E. Q.; Vakarelski, I. U.; Chan, D. Y. C.; Thoroddsen, S. T. Stabilization of Thin Liquid Films by Repulsive van der Waals Force. *Langmuir* **2014**, *30*, 5162−5169.
(46) Philipse, A. P.; Vrij, A. Preparation and Properties of Nonaqueous Model Dispersions of Chemically Modified, Charged Silica Spheres. *J. Colloid Interface Sci.* **1989**, *128*, 121−136.
(47) Rayss, J.; Sudolski, G. Ion Adsorption in the Porous Sol-Gel Silica Layer in the Fiber Optic pH Sensor. *Sens. Actuators, B* **2002**, *87*, 397−405.
(48) Parks, G. A. The Isoelectric Points of Solid Oxides, Solid Hydroxides, and Aqueous Hydroxo Complex Systems. *Chem. Rev.* **1965**, *65*, 177−198.
(49) Lee, S. H.; Rusakova, I.; Hoffman, D. M.; Jacobson, A. J.; Lee, T. R. Monodisperse $SnO_2$-Coated Gold Nanoparticles Are Markedly More Stable than Analogous $SiO_2$-Coated Gold Nanoparticles. *ACS Appl. Mater. Interfaces* **2013**, *5*, 2479−2484.